Nuclear Engineering and Technology 52 (2020) 841–845

Contents lists available at ScienceDirect

Nuclear Engineering and Technology

journal homepage: www.elsevier.com/locate/net

Original Article

Optimization of airborne alpha beta detection system modeling using MCNP simulation

Si Hyeong Sung, Hee Reyoung Kim*

Nuclear Engineering, Ulsan National Institute of Science and Technology, 50, UNIST-gil, Ulsan, 44919, Republic of Korea

ARTICLE INFO

Article history:
Received 26 April 2019
Received in revised form
3 October 2019
Accepted 8 October 2019
Available online 9 October 2019

Keywords:
PIPS detector
MCNP6
Semiconductor detector
Modeling
Resolution
FWHM

ABSTRACT

An airborne alpha beta detection system using passivated implanted planar silicon (PIPS) detector was modeled with the MCNP6 code and its resolution and detection efficiency were analyzed. Simulation of the resolution performed using the Gaussian energy broadening (GEB) function showed that the full width at half maximum (FWHM) of 35.214 keV for alpha particles was within 34–38 KeV, which is the FWHM range of the actual detector, and the FWHM of 15.1 keV for beta particles was constructed with a similar model to 17 keV, which is the FWHM range of an actual detector. In addition, the detection efficiency and the resolution were simulated according to the distance between the detector and the air filter. When the distance was decreased to 0.2 cm from 0.8 cm, the efficiency of the alpha and beta particles detection decreased from 5.33% to 4.89% and from 5.64% to 4.27%, respectively, and the FWHM of the alpha and beta particles improved from 40.9 KeV to 29.84 keV and 25.76 keV–13.27 keV, respectively.

1. Introduction

Alpha and beta spectrometry are widely used to analyze environmental radiation measurements and to identify the presence of alpha and beta emission radionuclides [1]. Owing to the characteristics of alpha and beta particles, the spectrum measurement is conducted in a vacuum environment, essentially to prevent the continuous energy loss caused by their interaction with the medium [2]. Consequently, it is necessary to prepare a thin and uniform source of the sample by performing radiochemical pretreatment followed by radiochemical separation and a deposition process such as electrodeposition and microprecipitation [3]. However, it is difficult to measure the radiation doses for workers in real time and to guarantee radiation protection in the work environment.

In this study, detector simulation is performed using a passivated implanted planar silicon (PIPS) detector to develop a mobile system for the real-time measurement of alpha and beta radioactive nuclides in air. In the proposed system, a radionuclide aerosol sample is collected from an air filter, which is then subjected to nuclide analysis and dose measurement using a PIPS detector. However, it is difficult to perform dose measurement because thick sources, such as aerosol, cause degradation of the energy resolution, which affects the quality of the alpha spectra containing several overlapping peaks. Additionally, the peak overlap due to radon and radon progeny in the air and natural background radiation is a major cause of the resolution degradation. Consequently, the MCNP simulation is performed to derive the optimized spectrum resolution of the airborne alpha beta detection system. The continuous air monitor (CAM) using PIPS detector is modeled using the MCNPX code [4], and the modeling of the PIPS detector for beta particles, which emitted the water sample response function using MCNP5, is performed [5]. In this study, the simulation program uses the MCNP6 code that can simulate complex geometry constructions, visualization tools, and functions of various particle transport physics models [6,7]. A PIPS detector model suitable for the airborne alpha–beta detection system under consideration is selected, and a simulation is built based on the information of the detector. The modeling of the PIPS detector resolution was optimized similar to the actual resolution performance. The resolution of PIPS detector was also optimized. Furthermore, changes in the resolution and detection efficiency according to the position of the detector and filter were analyzed.

* Corresponding author.
E-mail address: kimhr@unist.ac.kr (H.R. Kim).

https://doi.org/10.1016/j.net.2019.10.007

2. Materials

2.1. PIPS detector

When an externally incident particle is stopped in the depletion region of a PIPS detector, it forms electron—hole pairs, and the number of electron—hole pairs formed is directly proportional to the energy of the particle. The electric field of this region sweeps electrons to one terminal and holes to the other terminal [8]. The thickness of the depletion region depends on the bias voltage, and the higher the voltage, the higher the energy particles that can be stopped. This is called capacitance of the PIPS detector. Equation (1) represents capacitance of the detector and Equation (2) represents the depletion width [9].

$$C = \varepsilon \frac{A}{W} \tag{1}$$

$$W = \sqrt{2\varepsilon u \rho V} \tag{2}$$

where C is capacitance (pF), A is the active area (cm^2), W is the thickness (cm) of PIPS detector, ε is permittivity $\left(\frac{A \cdot s}{Vm}\right)$, u is mobility of majority charge carriers $\left(\frac{cm^2}{V \cdot s}\right)$, ρ is resistivity ($\Omega \cdot cm$) and V is bias voltage (V). The resulting charge pulse is integrated in the preamplifier to produce a voltage pulse. The larger the detector area, the wider the measurement range, the higher the detection efficiency, but the lower the resolution. Table 1 shows the performance changes of PIPS detector with changes in the active area for specifications based on Canberra's PIPS detector series [10]. It can be seen from the table that for the model with an active area of 450 mm^2, the full width at half maximum (FWHM) difference is 1.84 times larger for alpha particles and 1.76 times larger for beta particles than those for the model with an active area of 1700 mm^2. Although the detection efficiency can be improved by geometric adjustment of the filter and detector, the radiation peak discrimination performance is also essential for background removal in an aerosol sample measurement. Consequently, the simulation is performed using the model with an active area of 450 mm^2.

2.2. Computer simulation modeling

The simulation is performed using the MCNP6 general-purpose Monte Carlo code [11]. Initially, the structure of the system is simulated using the geometry function. Fig. 1 shows the conceptual diagram of the detection part of the airborne alpha—beta detector system and Fig. 2 shows schematic of detection system constructed using MCNP6. For the simulation geometry, the diameter of the PIPS detector is set to 23.9 mm and the height to 12.3 mm. The type of filter used is a cellulose—asbestos paper, and the diameter of the filter exposed to the detector is set to 50.0 mm and thickness to 0.2 mm. The detector is composed of stainless steel 304 surrounded by silicon that is exposed to air. The air filter consists of 19.1% of Si, 14.7% of Al, 2.9% of Mg, and 63.2% of O [12,13]. The PIPS detector is

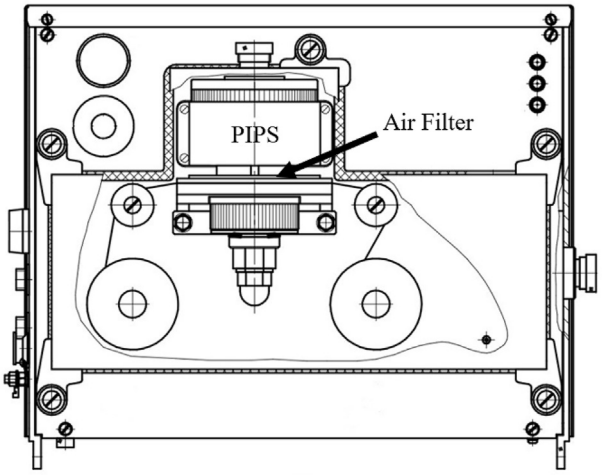

Fig. 1. Conceptual diagram of the detection part of the airborne alpha beta detector system.

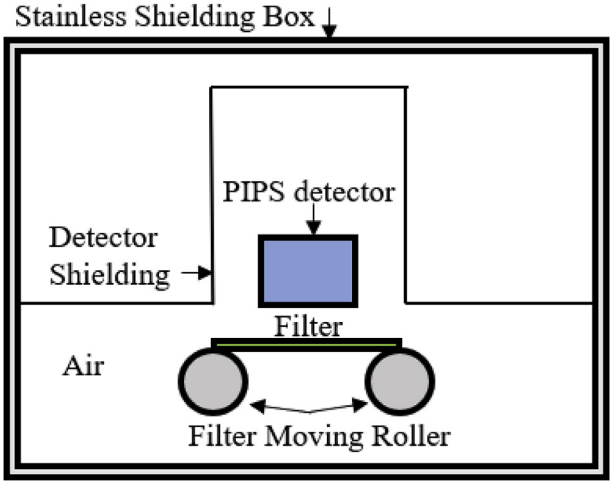

Fig. 2. Schematic of detection system in MCNP6.

located inside a box-shaped shield made of stainless steel 304, and the empty space is filled with air. The source is simulated as 0.3 μm of dust, randomly distributed inside the filter, and a random number is created using the MATLAB code. The source nuclides are ^{241}Am and ^{214}Pb, and the energy and abundance described in Table 2. In addition, the source information is input with reference to the ICRU report 56 [14]. The energy emitted from the source is represented in the form of a histogram, and the probability of the energy emission of each particle is inserted. The Physics model uses the F8 (pulse-height) tally to calculate the pulse—height value. With this card, the pulse height varies with the collection of particles. Furthermore, the energy cut-off is used as the variance reduction technique, which implies that particles whose energy is

Table 1
Canberra CAM PIPS detector performance.

Model	CAM450	CAM600	CAM900	CAM1200	CAM1700
Active area (mm^2)	450	600	900	1200	1700
Active diameter (mm)	23.9	27.6	33.9	39.1	46.5
Height (mm)	12.3	12.3	12.3	12.3	12.3
Alpha resolution (FWHM-in keV)	34–38	37–42	39–45	45–55	55–70
Beta resolution (FWHM-in keV)	17	20	22	25	30

Table 2
Energy and abundance about ^{241}Am and ^{214}Pb Source.

^{241}Am E (keV)	α Abundance (%)	^{214}Pb (keV)	β Abundance (%)
4757.39	0.00004	9.5	0.0002
4800.62	0.00086	53.2275	0.0004
4834.15	0.0007	56.84	0.015
4888.9	0.0007	62.7	0.015
4956.0	0.0007	107.22	0.015
4961.6	0.0007	118.16	0.015
4963.63	0.0007	137.45	0.006
5007.58	0.0001	141.3	0.004
5055.34	0.0001	170.07	0.032
5066.22	0.00014	181.5	0.032
5092.05	0.0004	196.20	0.069
5099.09	0.0004	205.68	0.0115
5106.71	0.0004	216.47	0.022
5117.20	0.0004	238.4	0.015
5133 *4*	0.0004	241.997	7.43
5155.16	0.0007	258.87	0.524
5179.34	0.0003	274.80	0.474
5181.64	0.0009	295.224	19.3
5190.4	0.0006	298.76	0.02
5217.27	0.0006	305.26	0.031
5225.08	0.0013	314.32	0.078
5232.5	0.0013	323.83	0.028
5244.12	0.0024	351.93	37.6
5281.01	0.0005	462.00	0.221
5321.90	0.015	480.43	0.320
5388.23	1.6	487.09	0.422
5416.27	0.01	511.0	0.032
5442.80	13.0	533.66	0.186
5469.45	0.04	538.41	0.020
5485.56	84.5	543.81	0.069
5511.47	0.22	580.13	0.352
5544.5	0.34	765.96	0.078
		785.96	1.07

out of the range of interest are terminated so that the computation time is not wasted following them.

3. Results and discussion

3.1. FWHM

To evaluate the accuracy of the PIPS detector, we compared the FWHM value obtained from the simulation results with the specifications of the commercially used PIPS detector with an active area of 450 mm^2. The F8 tally uses the Gaussian energy broadening (GEB) function was applied to adjust the FWHM of the simulation detector. The GEB parameter specifies the FWHM of the observed energy broadening in a physical radiation detector. The GEB feature also simulates the peak-broadening effects exhibited by the physical radiation detectors using Equation (3).

$$\mathrm{FWHM} = a + b\sqrt{E + cE^2} \tag{3}$$

(a = 5.797E-4 MeV, b = 7.192E-4 MeV$^{1/2}$, c = 1.0 MeV^{-1}).

For this tally card, the parameters a, b, and c are set, where E is the particle energy. The simulations are repeated to obtain the GEB values that yield the similar FWHM results as of the modeling PIPS detector. The tested GEB values vary from 10 keV to 200 keV. The GEB cards are used to perform Gaussian broadening on tally values [15]. In this evaluation, the distance between the filter and the detector was set to 0.4 cm, the alpha calibration source was ^{241}Am, and the beta calibration source was ^{214}Pb. The FWHM of the measured spectrum was calculated using the ORIGIN software, setting the peak based on the information of each source. The standard deviation was obtained from the Gaussian equation as shown in Equation (4), and the calculated value was substituted into Equation (5) to obtain the FWHM [16].

$$f(x) = \frac{1}{\sigma\sqrt{2\pi}} \exp\left[-\frac{(x - x_0)^2}{2\sigma^2}\right] \tag{4}$$

$$\mathrm{FWHM} = 2\sqrt{2ln2}\sigma \approx 2.3548200\sigma \tag{5}$$

In this equation, σ is the standard deviation and x_0 is the mean value of the function. Figs. 3 and 4 show the ^{241}Am spectrum graph and the ^{214}Pb spectrum graph, respectively. The peak is formed at 5.486 MeV for ^{241}Am, and at 0.728 MeV for ^{214}Pb according to the radionuclide decay. Consequently, it can be confirmed that the PIPS detector modeling works as expected. ^{241}Am and ^{214}Pb were used as the calibration sources and the GEB parameter was repeatedly applied. The FWHM value for each GEB parameter was calculated and the process was repeated till the specification of a commercial detector was achieved. Tables 3 and 4 show the FWHM calculation values according to the GEB repetition when using ^{241}Am and ^{214}Pb, respectively. The FWHM calculations were performed for ^{241}Am and ^{214} Pb at 5.486 MeV peak and 0.728 MeV peak, respectively. The FWHM value of alpha particle was 35.214 keV, which is considered to satisfy the performance of the PIPS detector as the simulation target. The FWHM value of beta particle was 15.1 keV, which is similar to that of a commercial PIPS detector. However, it is necessary to perform additional iterative simulations to produce a precise detector pulse.

3.2. Resolution and detection efficiency

The detection efficiency and the resolution were simulated according to the distance between the detector and the air filter. The distance between the detector and the filter was varied, and set to 0.2 cm, 0.4 cm, 0.6 cm, and 0.8 cm to perform the simulation. ^{241}Am and ^{212}Bi were used as the target nuclides for alpha and beta particles, respectively [17]. To derive the detection efficiency, the MCNP calculated value of the particle detection probability of the PIPS detector is multiplied by the activity of the nuclide, and then this product is divided by the number of alpha particles produced, as shown in Equation (6).

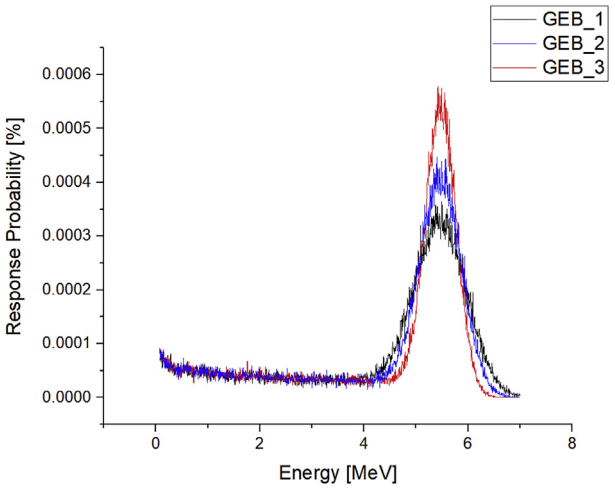

Fig. 3. ^{241}Am spectrum graph according to repeat GEB function.

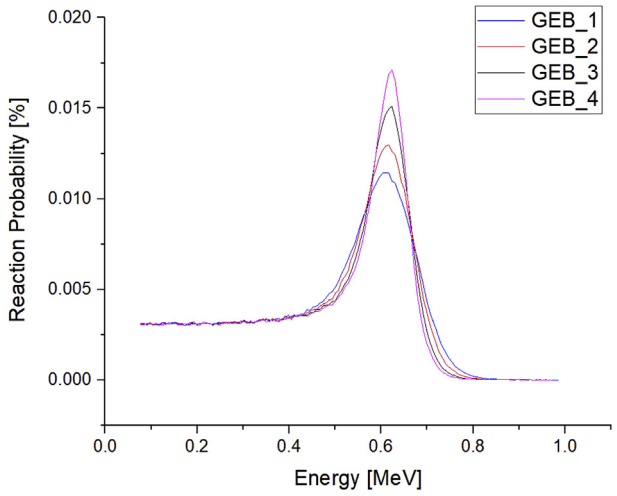

Fig. 4. ^{214}Pb spectrum graph according to repeat GEB function.

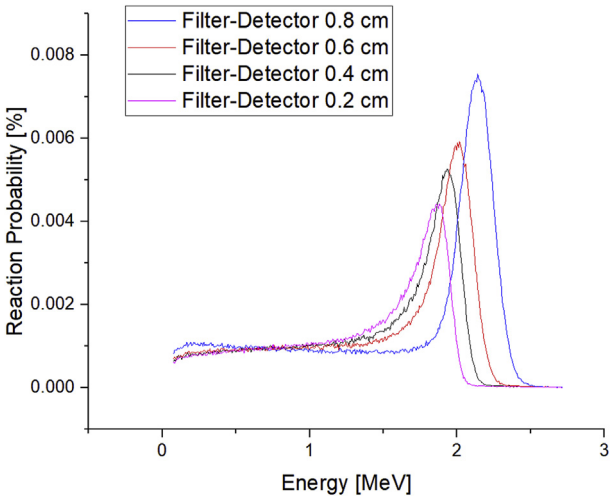

Fig. 6. ^{212}Bi spectrum graph according to distance from air filter to detector.

Table 3
Alpha FWHM calculation according to GEB case.

GEB Case	Peak [MeV]	FWHM [keV]	Nominal FWHM [keV]
1	5.486	68.275	34–38
2	5.486	52.154	34–38
3	5.486	35.214	34–38

Table 4
Beta FWHM calculation according to GEB case.

GEB Case	Peak [MeV]	FWHM [keV]	Nominal FWHM [keV]
1	0.728	36.6	17
2	0.728	24.7	17
3	0.728	15.1	17
4	0.728	9.14	17

$$\text{Detection Efficiency}(\varepsilon) = \frac{T\# \times A}{P\#} \quad (6)$$

(T # = tally, A = source activity, P # = Total number of emitted particle).

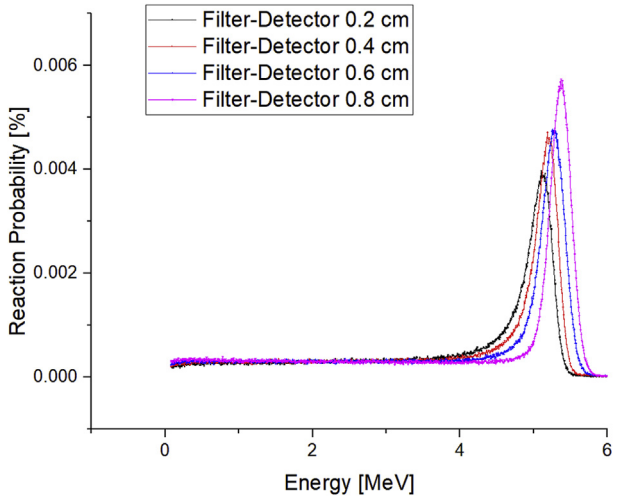

Fig. 5. ^{241}Am spectrum graph according to distance from air filter to detector.

Figs. 5 and 6 represent the alpha and beta spectra according to the distance, respectively. It was confirmed that the peak FWHM was narrow and the count rate increased as the distance between alpha and beta particles decreased. Since the probability of alpha and beta particles reacting with air is low, the resolution and the count rate increased as the probability of these particles entering the detector increased. Table 5 shows the computed values of the detection efficiency and FWHM. The detection efficiencies of alpha and beta particles decreased from 5.33% to 4.89%, and from 5.64% to 4.27%, respectively, for a distance change from 0.2 cm to 0.8 cm. When the detector was placed at a distance of 0.2 cm from the air filter, it was confirmed that the detection efficiency decreased by 0.44% and FWHM of alpha particles increased by 11.06 keV, respectively, as compared to the case where the detector was located at a distance of 0.8 cm. In the case of beta particles, the detection efficiency decreased by 1.37% when detector moved from 0.2 cm to 0.8 cm, otherwise FWHM of beta particles increased by 12.49 keV. The decrease in resolution due to the increase in efficiency is clearly shown. As a result, it was confirmed that the distance between the source and the detector is 0.4 cm, which is a suitable performance. It is necessary to consider the correlation between detector resolution and efficiency. Therefore, an alpha–beta detection system optimized for spectrum analysis should be designed, considering the resolution and detection efficiency according to the distance between detector and source.

4. Conclusion

To construct an airborne alpha—beta detection system, a PIPS detector was modeled using the MCNP6 code that can simulate its detection efficiency and resolution for various situations. The resolution of the PIPS detector was modeled with similar performance to an actual detector. The results of resolution modeling of the detector showed that the FWHM was 97.2% similar to the performance of actual detector, with values of 35.214 keV for alpha and 16.569 keV for beta particles. As a result of modeling of the airborne alpha beta detection system using the air filter and PIPS detector, it was confirmed that the detection efficiency and FWHM are optimized when the distance between the source and the detector is 0.4 cm. Based on the optimized simulations of the airborne alpha–beta detection system presented in this study, the basis for the feasibility of the detection system was established.

Table 5
Alpha and beta detection efficiency and FWHM.

Case	Detection Efficiency (%)	FWHM [keV]	Case	Detection Efficiency (%)	FWHM [keV]
Alpha_0.2 cm	5.33±0.1	40.90	Beta_0.2 cm	5.64±0.11	25.76
Alpha_0.4 cm	5.20±0.08	36.26	Beta_0.4 cm	5.03±0.07	18.29
Alpha_0.6 cm	5.05±0.09	32.15	Beta_0.6 cm	4.65±0.07	16.43
Alpha_0.8 cm	4.89±0.08	29.84	Beta_0.8 cm	4.27±0.0.9	13.27

Declaration of competing interest

The authors declare that they have no known competing financial interests or personal relationships that could have appeared to influence the work reported in this paper.

Acknowledgments

This work was supported by the National Research Foundation of Korea (NRF) grant funded by the Korean government (MSIP: Ministry of Science, ICT and Future Planning) NRF-22A20153413555.

This work was supported by the 'Development of Portable Radioactive Contamination Monitoring System for Alpha and Beta Dust Source in the Air' of the Korea Institute of Energy Technology Evaluation and Planning (KETEP) granted financial resource from the Ministry of Trade, Industry & Energy, Republic of Korea (No. 20171510300590).

Nomenclature

C	Capacitance (pF)
A	Active area (cm^2)
W	Thickness of depletion region (cm)
ε	Permittivity $\left(\frac{A \cdot s}{V \cdot cm}\right)$
u	Mobility of majority charge carriers $\left(\frac{cm^2}{V \cdot s}\right)$
ρ	Resistivity ($\Omega \cdot$cm)
V	Bias voltage (V)
σ	Standard deviation
x_0	Mean value of the function
T #	Tally number
A	Source activity
P #	Total umber of emitted particle

Appendix A. Supplementary data

Supplementary data to this article can be found online at https://doi.org/10.1016/j.net.2019.10.007.

References

[1] E. Garcia-Torano, Current status of alpha-particle spectrometry, Appl. Radiat. Isot. 64 (2006) 1273–1280.
[2] R. Kierepko, J.W. Mietelski, Z. Ustrnul, R. Anczkiewicz, H. Wershofen, Z. Holgye, et al., Plutonium isotopes in the atmosphere of Central Europe: isotopic composition and time evolution vs. circulation factors, Sci. Total Environ. 569 (2016) 937–947.
[3] Robert B. Hayes, Craig M. Marianno, Use of MCNPX for alpha spectrometry simulations of a continuous air monitor, Trans. Am. Nucl. Soc. 96 (2007) 631–633.
[4] M.K. Pham, J.J. La Rosa, S.-H. Lee, B. Oregioni, P.P. Povinec, Deposition of Saharan dust in Monaco rain 2001–2002: radionuclides and elemental composition, Phys. Scr. T118 (2005) 14–17.
[5] Grujic Selena, Milosevic Miodrag, Uranija Kozmidis-Luburic, Bikit Istvan, Mont Carlo simulation of beta radiation response function for semiconductor Si detector, Nucl. Instrum. Methods Phys. Res. Sect. A Accel. Spectrom. Detect. Assoc. Equip. 654 (2011) 288–292.
[6] T. Siiskonen, R. Pöllänen, Advanced simulation code for alpha spectrometry, Nucl. Instrum. Methods Phys. Res., Sect. A 550 (2005) 425–434.
[7] L.S. Waters, G.W. McKinney, J.W. Durkee, M.L. Fensin, J.S. Hendricks, M.R. James, et al., The MCNPX Monte Carlo radiation transport code, in: AIP Conference 2007, 2007, pp. 81–90.
[8] C. Yang, D.N. Jamieson, S.M. Hearne, C.I. Pakes, B. Rout, E. Gauja, et al., Ion-beam-induced-charge characterisation of particle detectors, Nucl. Instrum. Methods Phys. Res., Sect. B 190 (2002) 212–216.
[9] M. Krammer, Silicon Detectors, HEPHY, Institute of High Energy Physics, Praktikum, 2011.
[10] Passivated Implanted Planar Silicon (PIPS) Detectors, Product Catalogue, U.S.A., Canberra Industry, 2008.
[11] MCNP6 User's Manual. LA-CP-13-00634, Version 1.0, Los Alamos National Laboratory Report, California, 2013.
[12] R. Hayes, A.M. Peña, T.E. Goff, Use of alpha spectroscopy for conducting rapid surveys of transuranic activity on air sample filters and smears, Health Phys. 89 (2005) 172–180.
[13] reportA State of the Art on the Technology for Downgrading and Volume Reduction of Radioactive HEPA Filter Waste, KAERI/AR-861/2010, Korea Atomic Energy Research Institute Report, Daejeon
[14] Dosimetry of External Beta Rays for Radiation Protection, ICRU REPORT 56, International Commission on Radiation Units and Measurements, U.S.A., Bethesda, Maryland, 1997.
[15] S. Ihantola, A. Pelikan, R. Pöllänen, H. Toivonen, Advanced alpha spectrum analysis based on the fitting and covariance analysis of dependent variables, Nucl. Instrum. Methods Phys. Res., Sect. A 656 (2011) 55–60.
[16] R. Pöllänen, T. Siiskonen, High-resolution alpha spectrometry under field conditions e fast identification of alpha particle emitting radionuclides from air samples, J. Environ. Radioact. 87 (2006) 279–288.
[17] In Situ Leaching of Uranium Technical, Environmental and Economics Aspects, International Atomic Energy Agency, Vienna, 1989. IAEA-TECDOC-492.